Effect of electric field polarization and temperature on the effective permittivity and conductivity of porous anodic aluminium oxide membranes

Alessio Tamburrano [a,*], Biagio De Vivo [b], Magnus Höijer [c], Laurent Arurault [d], Vincenzo Tucci [b], Sandra Fontorbes [d], Patrizia Lamberti [b], Virginie Vilar [d], Barbara Daffos [d], Maria Sabrina Sarto [a]

[a] Sapienza University of Rome, Research Center for Nanotechnology Applied to Engineering (CNIS), 00184 Rome, Italy
[b] University of Salerno, Department of Electronic and Computer Engineering, 84084 Fisciano (SA), Italy
[c] Swedish Defence Research Agency FOI, Information Systems, SE-581 11 Linköping, Sweden
[d] Université de Toulouse, CIRIMAT, UPS/INPT/CNRS, LCMIE, 31062 Toulouse Cedex 9, France

A B S T R A C T

Porous insulators offer new opportunities for the controlled guest–host synthesis of nanowires for future integrated circuits characterized by low propagation delay, crosstalk and power consumption. We propose a method to estimate the effect of the electric field polarization and temperature on the electrical properties of different types of synthesized porous anodic aluminium oxide membranes. It results that the effective permittivity along the pore axis is generally 20% higher than the one in the orthogonal direction. The type of solution and the voltage level applied during anodization are the main parameters affecting the AAO templates characteristics, i.e. their porosity and chemical content. The values of permittivity of the final material, are typically in the range 2.6–3.2 for large pore diameter membranes including phosphorus element and having a low water content, and in the range 3.5–4 for the ones with smaller pores, and showing sulphur element incorporation. Moreover, the dc conductivity of the different membranes appears to be correlated to the pore density.

Keywords:
Anodic aluminium oxide membrane
Electrical and electromagnetic properties
Electromagnetic modelling
Complex permittivity measurement

1. Introduction

Anodic aluminium oxide (AAO), due to their peculiar characteristics such as controllable pore shape and distribution have received considerable attention for the realization of templates in which nanostructure formation can take place by self-organizing methods [1,2]. Carbon nanotubes (CNTs) grown inside such templates have been proposed to realize large scale interconnects for future Ultra Large Scale Integration (ULSI) circuits [3]. A wide investigation on the synthesis, fabrication, characterization and modelling of CNT–AAO composite for next-generation nanointerconnects have been performed during the last three years within the European project CATHERINE (www.catherineproject.eu). Due to their remarkable mechanical and thermal properties, the AAO templates in which CNT structures are grown can also represent a structural support for interconnects. In order to design reliable CNTs-based interconnects, the electrical properties of the AAO support must be properly taken into account since they can affect the electromagnetic response of the device.

Although a large amount of data exists concerning the morphological and structural properties of the porous AAO membranes and the relations between the pores characteristics and the parameters of the fabrication process, a similar broad range of information is not available concerning the electric properties of such materials and their dependence on the operating conditions [4–6]. Therefore, a specific and detailed characterization activity has been performed in our group aimed at measuring the low frequency electrical conductivity and permittivity of AAO templates as a function of the applied electric field and temperature. In particular, it is investigated how the electric field polarization affects the values of the effective permittivity of different types of AAO membranes experimentally prepared or commercially available.

Due to the characteristics of the AAO templates, i.e. the high fragility and their thickness in the range 10–100 μm, the measurement of the electrical properties is performed in general applying an electric field parallel to the pore axis as described in the standard ASTM D150 [9]. Therefore, both the electrical conductivity and the effective permittivity are obtained along this direction. In order to extract the effective complex permittivity of the AAO template also in the direction orthogonal to the pores, the homogenization theory is applied. At first, the porous material is modelled in the presence of an electric field parallel to the pores in order to extract from the measured effective permittivity the

* Corresponding author. Address: Sapienza University of Rome, Research Center for Nanotechnology Applied to Engineering (CNIS), Via Eudossiana 18, 00184 Rome, Italy. Tel.: +39 0644585803; fax: +39 064883235.
E-mail address: alessio.tamburrano@uniroma1.it (A. Tamburrano).

doi:10.1016/j.mee.2011.08.007

corresponding values for the bulk aluminium oxide constituting the membrane. Then, the AAO template is simulated in the case the electric field is directed orthogonally to the pores, and the corresponding effective permittivity value is computed starting from the extracted bulk properties.

2. Experimental

2.1. Sample preparation

Three different types of AAO porous templates were prepared, using repeatable processes previously studied and extensively tested [7,8].

The substrates were always pure aluminium (99.99%), whereas all used chemical compounds were analytical grade and aqueous solutions were obtained using deionised water.

The first type (F1) was an AAO porous film supported on aluminium foil. Five F1 samples were prepared, starting from an aluminium substrate (50 mm in diameter and 100 μm thick) electropolished at 25 V for 2 min in a Jacquet mixed solution. Anodizing was carried out for 8 h at 152 V by an INVENSYS LAMBDA generator (300 V – 5A). The electrolyte was made up of an aqueous phosphoric acid solution (8 wt.%), while a pure aluminium plate (99.99%) was used as cathode. The temperature was regulated at −1.5 °C by a cryostat (HUBER CC2). The supported anodic film was then immersed for 30 min in a phosphoric acid solution (8 wt.%) and then rinsed with deionised water.

The second type (F2) was a stand-alone AAO membrane with large pores; five F2 samples were prepared. The preparation process of the AAO templates with large pores was described elsewhere [7,8]. The aluminium substrate (14 mm in diameter and 2 mm thick) was prepared first by sanding, then by annealing under N_2 atmosphere at 450 °C for 2 h, finally by an electropolishing. Anodizing was performed at 185 V for 4 h using a phosphoric acid solution. After growth of the porous anodic film, a removal of the compact layer was performed using 30 V AC voltage (Universal Power Supply EA-4036) in a phosphoric acid solution and then the substrate was chemically dissolved using a hydrochloric acid solution (18 wt.%) including copper chloride (0.1 mol/L). The membrane was then immersed for 5 min in a phosphoric acid solution and finally rinsed with deionised water.

The third type (F3) was a stand-alone AAO membrane with small pores. One membrane was studied here. The pre-treatments of the substrate and the removal of the compact layer were similar to those performed for the F2 membranes. The main difference was that anodizing was performed for 5 h at 28 V in sulphuric acid solution (0.3 M).

As comparison, three stand-alone commercial membranes (anodisc; sample diameter: 13 mm and 47 mm; pores diameter: 200 nm) manufactured by Whatmann were also studied.

2.2. Microscope and chemical analysis

Field Emission Gun Scanning Electron Microscope (FEG-SEM JEOL JSM 6700F) was used to determine the microstructure of the templates, i.e. the pores density (ρ), the pore diameter (D), the thickness of the porous layer (e_p), the percentage of the void volume (τ) and the interdistance between the axis of two adjacent pores (B). FEG-SEM was coupled with an energy dispersive X-ray (EDX) spectrometer, enabling chemical elementary analysis.

X-ray diffraction (XRD) analysis was performed with a Bruker AXS D4 ENDEAVOR generator with copper anticathode (K_α = 1.5418 Å). All diffraction profiles were obtained by varying 2θ from 10° to 100°. Finally peaks were identified by using the EVA software.

The samples dehydration was studied by thermogravimetric analysis (TGA) in nitrogen 4.5 ($\geqslant$99.995 vol.%) from 25 to 110 °C at a heating rate of 10 °C/min., by using a SETARAM instrument (Model TAG 92 equipped with a platinum crucible).

The infrared spectroscopy (IRS) was performed using an IR-TF NICOLET 510P device, the spectra being recorded in transmission conditions between 400 and 4000 cm^{-1}. The F2 and F3 templates were preliminarily reduced in powder and prepared in KBr pellets. Notice that it was impossible to perform the IRS characterizations on F1 templates because the extremely thin thickness (16 μm) of the AAO film does not guarantee enough powder after the removal of the aluminium substrate to prepare suitable pellets.

2.3. DC conductivity and ac complex permittivity

The permittivity describes how a dielectric material reacts on an applied electric field. For an anisotropic material, like an AAO membrane, the permittivity tensor ε relates the electric displacement field vector **D** and the electric field vector **E**:

$$\mathbf{D} = \varepsilon \mathbf{E} \tag{1}$$

By choice of the co-ordinate axes according to Fig. 1, it results that for an AAO template the permittivity tensor assumes a diagonal form:

$$\varepsilon = \varepsilon_0 \begin{pmatrix} \varepsilon_h & 0 & 0 \\ 0 & \varepsilon_h & 0 \\ 0 & 0 & \varepsilon_z \end{pmatrix} \tag{2}$$

in which ε_0 is the free-space permittivity, ε_h and ε_z are the effective relative permittivity of the membrane when the applied electric field is directed along the x- or y-axis, and the z-axis, respectively. In general both quantities ε_h and ε_z are complex and can be expressed as function of the effective ac (alternating current) real permittivity (ε'_h and ε'_z), and of the effective ac electrical conductivity (σ_h and σ_z):

$$\varepsilon_h = \varepsilon'_h + \sigma_h/(j\omega\varepsilon_0) \tag{3a}$$

$$\varepsilon_z = \varepsilon'_z + \sigma_z/(j\omega\varepsilon_0) \tag{3b}$$

ω being the angular frequency. For $\omega = 0$, σ_h and σ_z represent the dc (direct current) electrical conductivity of the material. Due to the characteristics of the AAO templates, i.e. thickness in the range 10–100 μm and the high fragility, the effective permittivity can be measured only in the z-direction using standard methods. In the

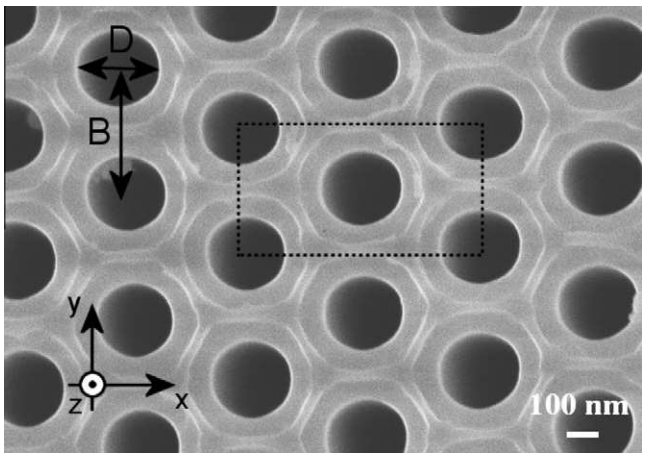

Fig. 1. FEG-SEM plan view of a typical F2 membrane. Diameter of pores (D) and distance between pores (B) denoted. The dashed line surrounds a unit cell of the membrane.

following it is described how the value of ε_h can be obtained by modelling, starting from measurements of ε_z.

2.4. Measurement of σ_z and ε'_z

The dc electrical conductivity σ_z of the AAO template has been obtained by using a voltage generator FUG HCN 35-6500 (max. output current 5 mA) and a picoammeter Keithley 6514 (min. current 10^{-15} A). In order to remove physisorbed water and ensure that measurements are performed on different specimens in the same conditions, each sample has been kept at 60 °C in oven for one day before testing. The measurements have been performed in five different positions over the sample surface in order to average the effect of local inhomogeneity.

The test procedure applied for the measurement of the effective complex permittivity ε_z is based on the capacitive method, as described in the ASTM D150 [9]. The standard provides guidance for choices of electrodes, apparatus and measurement techniques to asses the relative permittivity and dissipation factor of solid electrical insulating materials from few Hz to several hundred megahertz. In particular, the adopted measurement set-up entails sandwiching a thin sheet of the material under test between two metallic electrodes of a parallel plate capacitor. The test fixture is equipped with a 4-terminal pair cable assembly, guarded/guard electrodes, and a Mitutoyo micrometer to set the distance between the electrodes. The cable assembly is connected directly to the 4-BNC terminal pair of an Agilent 4294A precision impedance analyzer, and the configuration is changed to a 3-terminal at the guarded/guard electrodes. The use of a guard electrode has practically the aim of eliminating the fringing and stray capacitance at the edge of the guarded electrode from the measurement reading, enhancing the test accuracy. The adopted system allows to measure the dielectric properties of a material in the frequency range from 40 Hz up to 30 MHz. Calibration of the experimental set-up is also performed in order to reduce the residual impedance and stray admittance in the test fixture by measuring open and short standards and applying error correction functions.

The effective complex permittivity is then derived measuring the capacitance C and the dissipation factor tan δ at different frequencies. In particular, the real part (ε'_z) of the effective complex relative permittivity and the effective ac conductivity (σ_z) of the material samples under test are calculated using the following expressions:

$$\varepsilon'_z = C\frac{t}{A\varepsilon_0}, \tag{4a}$$

$$\sigma_z = \frac{t}{A}\omega C \tan\delta \tag{4b}$$

where t is the average thickness of the AAO membrane and A is the area of the guarded electrode. For each sample, the values of ε'_z and σ_z are obtained at different temperatures and averaged over 10 repeated measurements.

2.5. Extraction of σ_h and ε'_h

The AAO membrane is modelled as an inhomogeneous material having a periodic spatial structure, characterized by a period much smaller than the minimum wavelength associated to the EM field excitation. Such hypothesis is widely valid in the frequency range of interest for nanointerconnect applications: for instance at the frequency of 50 GHz, it results that the free-space wavelength is 6 mm, whereas the period characterizing the AAO membrane considered in this study is always shorter than 1 μm. Therefore, the membrane can be modelled as an effective homogeneous material disk [10–16].

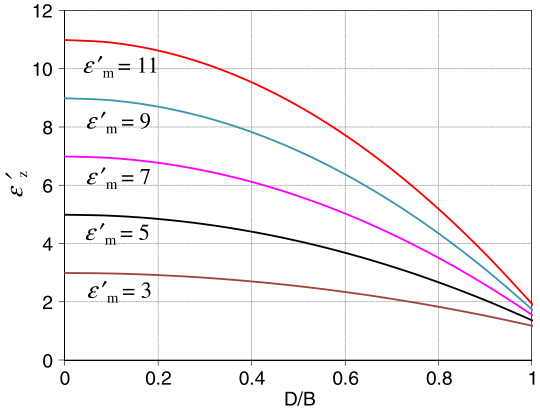

Fig. 2. Real part of the effective relative permittivity ε'_z as function of the diameter of the pores in the membrane when the field is directed parallel to the pore axis. The curves are drawn for increasing values of ε'_m.

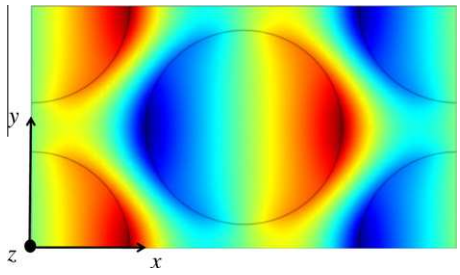

Fig. 3. Distribution of the normalized electric potential inside the unit cell of Fig. 1, in the case D/B = 80%.

In the case that the electric field is applied in the z-direction, the membrane acts macroscopically as two parallel coupled materials: the aluminium oxide of complex relative permittivity ε_m and air. The effective complex relative permittivity ε_z in (3b) is then expressed as function of the bulk complex permittivity ε_m:

$$\varepsilon_z = \tau + (1-\tau)\varepsilon_m \tag{5}$$

where τ is the volume fraction of the pores, which is given by:

$$\tau = \frac{\pi}{2\sqrt{3}}\left(\frac{D}{B}\right)^2 \tag{6}$$

D being the pore diameter and B the distance between the centres of two adjacent pores (Fig. 1).

The permittivity of the aluminium oxide surrounding the pores, ε_m, is extracted from (5), using the value of ε_z obtained from measurements as described in Section 2.4. As an example, Fig. 2 shows the real part of the relative permittivity along the z-axis (ε'_z) as function of the ratio D/B, for different values of the real part of the AAO relative permittivity (ε'_m).

Next, the relative effective permittivity of the membrane ε_h is calculated in the hypothesis that the field is applied in the x- or y-direction using the following expression [14,15]:

$$\varepsilon_h = \varepsilon_m\left[1 + \frac{\tau\beta(1-\varepsilon_m)}{\varepsilon_m - L\tau\beta(1-\varepsilon_m)}\right] \tag{7}$$

in which L = 0.5 is the source dyadic along the x- or y-axis of the circular cross-section of the pore [12], β is defined as the integral of the internal electric field along the x- or y-axis over the pore volume divided by its volume and by the external electric field along the same direction [15]. The exact electric field distribution in the unit cell of Fig. 1 can be computed from the electric potential distribution

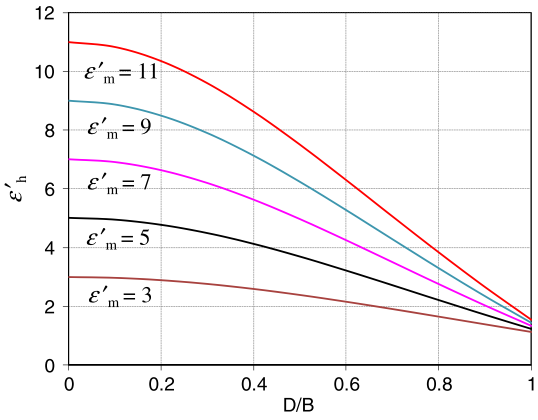

Fig. 4. Effective relative permittivity ε'_h as function of the diameter of the pores in the membrane when the field is directed in the plane of the membrane. The curves are drawn for increasing values of ε'_m.

shown in Fig. 3, obtained by solving numerically Laplace problem in the non-homogeneous material. However, if the thickness of the membrane is much greater than the pore diameter and distance, β can be approximated by the following analytical expression [15]:

$$\beta = \frac{2}{\varepsilon_m^{-1} + 1} \tag{8}$$

The quantities ε'_h and σ_h are then obtained from (3a).

As an example, Fig. 4 shows the real part of the relative permittivity along the z-axis (ε'_h) as function of the ratio D/B, for different values of the real part of the AAO relative permittivity (ε'_m).

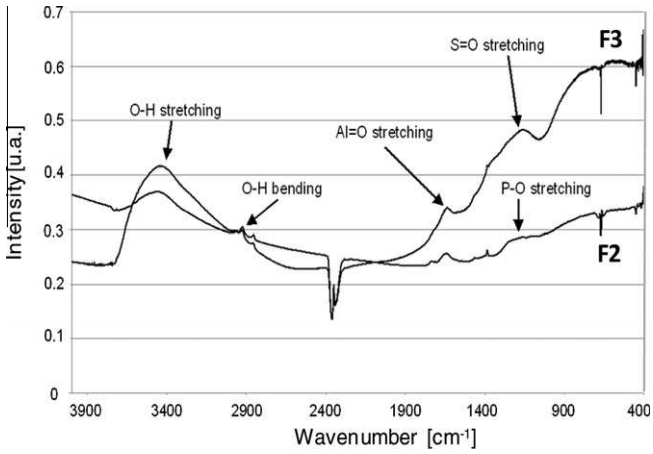

Fig. 6. Infrared spectra of membranes of type F2 and F3.

3. Results and discussions

3.1. Characterization of the anodic membranes before and after thermal treatment

The membranes were extensively characterized in order to know their microstructure and chemical composition just at the end of the preparation process but also after a thermal treatment at 110 °C. The results were then systematically compared with those obtained using the commercial membranes.

At the end of the preparation process, FEG-SEM images of F1, F2 and F3 membranes before thermal treatment show a well-defined

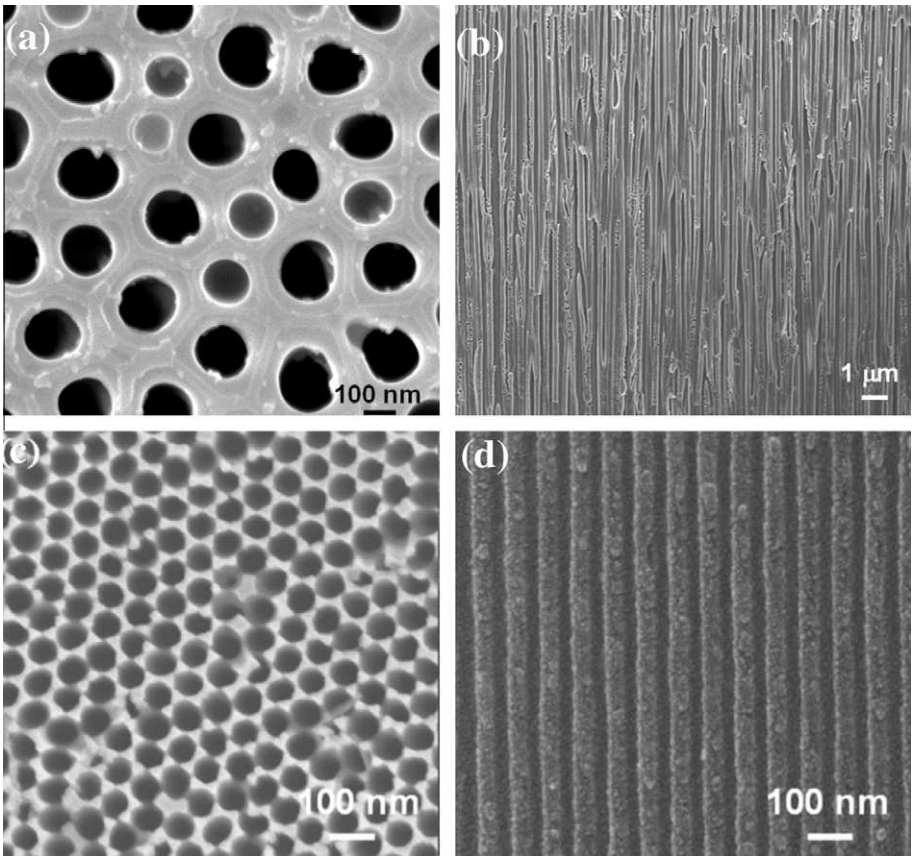

Fig. 5. FEG-SEM images of AAO templates: (a) plan view and (b) cross-section view of a typical membrane of family F1; (c) plan view and (d) cross-section view of a typical membrane of family F3.

Table 1
Average characteristics of the AAO templates.

Type	D (nm)	B (nm)	D/B	Pore density (m^{-2})	Thickness (μm)
F1	191 ± 19	299 ± 50	0.64	1×10^{13}	16
F2	254 ± 21	454 ± 44	0.56	7×10^{12}	60
F3	41 ± 11	66 ± 6	0.62	2×10^{14}	80
Commercial	273 ± 48	345 ± 86	0.79	9×10^{12}	60

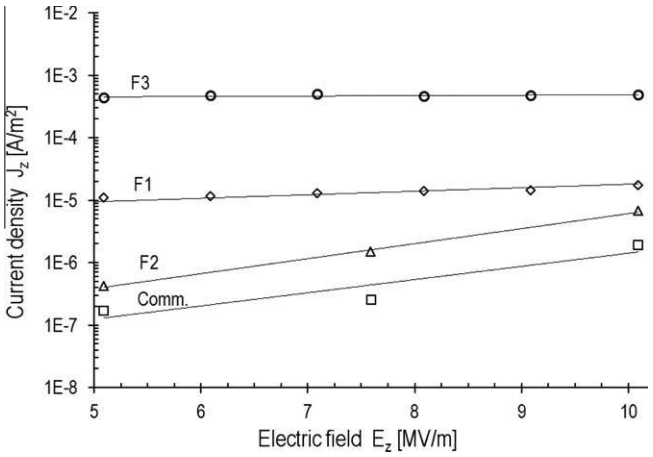

Fig. 7. Current density vs. applied electric field for all membranes at 110 °C.

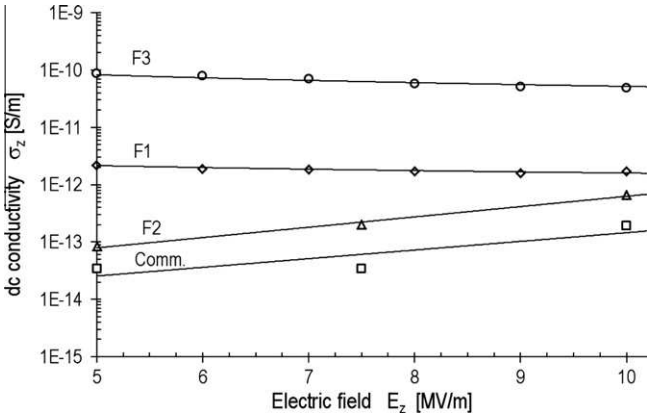

Fig. 8. Measured dc conductivity vs. electric field for all membranes at 110 °C.

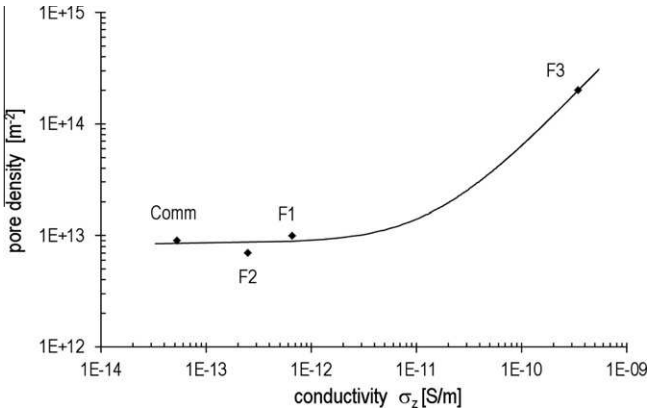

Fig. 9. Correlation between pore density and the dc conductivity under the highest value of the applied electric field.

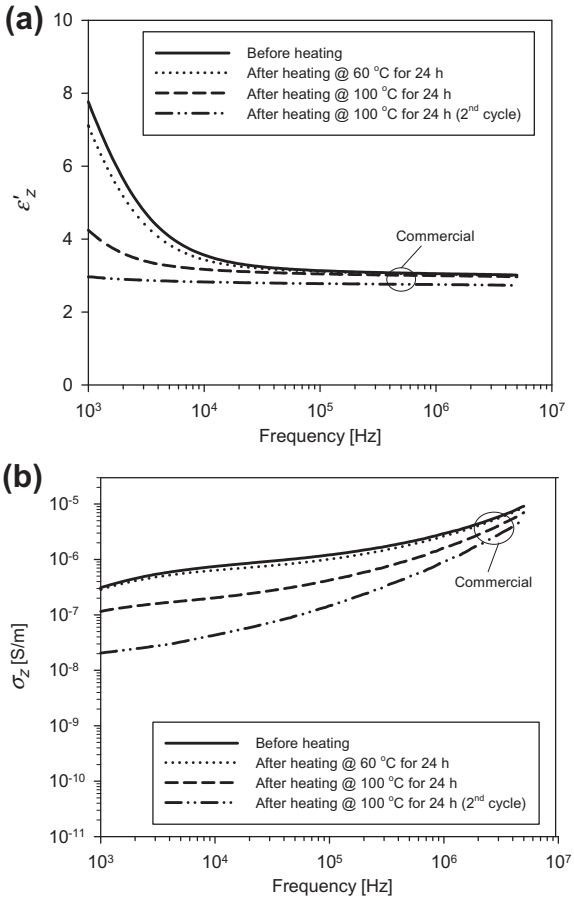

Fig. 10. Real part of the complex permittivity (a) and the effective ac conductivity (b) of the commercial AAO before and after thermal treatments.

microstructure, similar to Keller's model (Figs. 1 and 5(a)–(d)). The pores are parallel, straight and perpendicular to the initial metallic surface. Additional EDX analysis coupled with FEG-SEM qualitatively reveal the chemical elementary composition of the AAO templates, showing the presence of oxygen and aluminium.

The XRD results clearly show that all AAO membranes (research and commercial ones) are not made up of well-crystallized compounds, especially α-alumina, and are in fact amorphous in the 25–110 °C temperature range, i.e. despite our additional thermal treatments.

The IR spectra, reported in Fig. 6 for F2 and F3 membranes, highlight the presence of hydroxyl bonds and Al═O bond, indicating that research membranes are made up of aluminium hydrated (oxi)-hydroxide and amorphous hydrated oxide of aluminium. These results are in agreement with previous works [7,8], suggesting dehydration mechanisms of physisorbed (25–100 °C) and then chemisorbed water (100–800 °C) in AAO membranes. Furthermore, thermo-gravimetric analyses (TGA) specify that the water content increases 14-fold (from 0.07% to 1.00%) between F2 and F3 membranes.

Secondly, the EDX analyses show that F1 and F2 membranes, as well as the commercial ones, incorporate phosphorus element. In contrast, sulphur is characterized for F3 membranes. The IR spectra confirm these results because P–O and S═O stretching are showed, respectively, proving the incorporation of the anions coming from the anodizing electrolyte, i.e. phosphoric acid solution for all membranes, apart from Family 3 membranes prepared with sulphuric

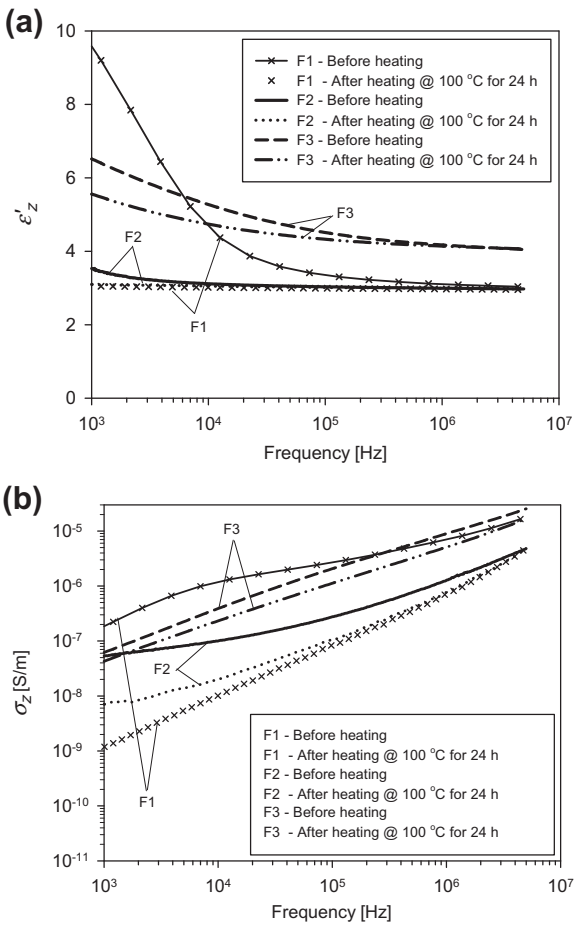

Fig. 11. Frequency spectra of ε'_z (a) and σ_z (b) of the AAO templates of type F1, F2, F3, having the characteristics reported in Table 1, before and after thermal treatment.

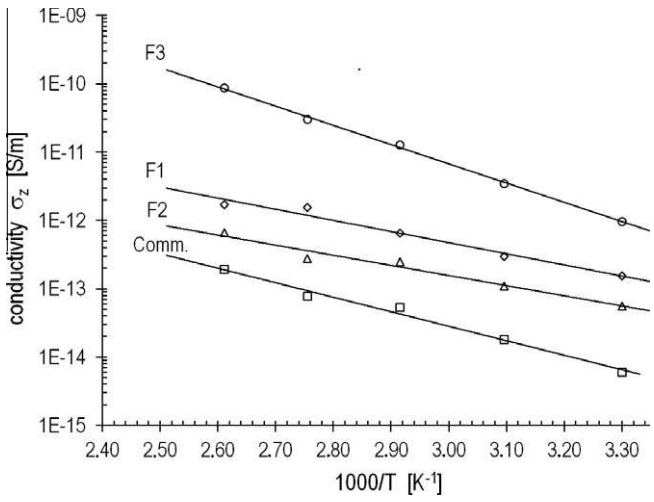

Fig. 12. Arrhenius plot of the dc conductivity for all membranes.

acid electrolyte. So the AAO templates are not made up of pure aluminium oxide but contain hydrated oxides, hydroxide and oxi-hydroxide of aluminium, as well as exogen anion coming from the anodizing electrolyte.

The presence of phosphorus or sulphur can change the crystallization phenomena of the allotropic crystallized phases of

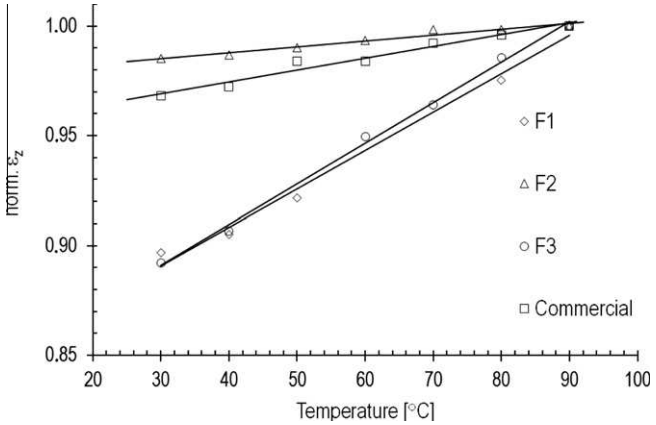

Fig. 13. Dependence of normalized relative permittivity ε'_z as function of the temperature at 1 MHz for all membranes. The normalization is performed with respect to the value measured at 90 °C (max temperature considered).

Table 2
Activation energy and permittivity temperature coefficient.

Type	E_a (eV)	$\Delta\varepsilon'_z/\Delta T$ (°C^{-1})
F1	0.27	4.1×10^{-3}
F2	0.28	1.4×10^{-3}
F3	0.48	2.3×10^{-2}
Commercial	0.37	1.5×10^{-3}

alumina, that appear nevertheless at high temperatures [17]. For example, the α-alumina phase (called corundum) usually requires thermal treatment at temperature higher than 1000 °C. This lack of crystallization in the 25–110 °C temperature range, is confirmed by the unchanged microstructures, showing the same pore diameter and porosity.

To sum up, it results that commercial, F1 and F2 membranes are similar from the chemical point of view, i.e. they contain phosphorus and a low level of water. In contrast, the F3 AAO templates are different due to the incorporation of sulphur and a higher water content. From the microstructure point of view, the research membranes show well-designed and ordered pores, in a large range of pore diameter as reported in Table 1. However, all membranes are mainly made up of aluminium hydrated (oxi)-hydroxide and amorphous hydrated oxide of aluminium, incorporating also anions coming from the anodizing electrolyte.

3.2. DC conductivity

The results of the dc characterization performed on all membranes are summarized in Figs. 7 and 8, where the values of the current density vs. applied electric field and the dc conductivity as a function of the applied field at 110 °C are reported. Several observations can be obtained from the analysis of such plots. In particular, it can be noticed that the commercial and the F2 membranes, characterized by similar morphological features (pore density and pore diameter) exhibit a comparable behaviour with a slight increase of the current and conductivity with the applied field. Moreover, also the values of the conductivity are similar to those reported in the literature for AAO membranes [18,19]. The membrane F1 shows an almost field independent conductivity with values, especially at low applied field, which are more than one order of magnitude higher than those of the commercial and F2 membranes. Since, as previously evidenced, F1 and F2 membranes have alike chemical composition and the main morphological difference is the number of pores per unit area, it can be argued

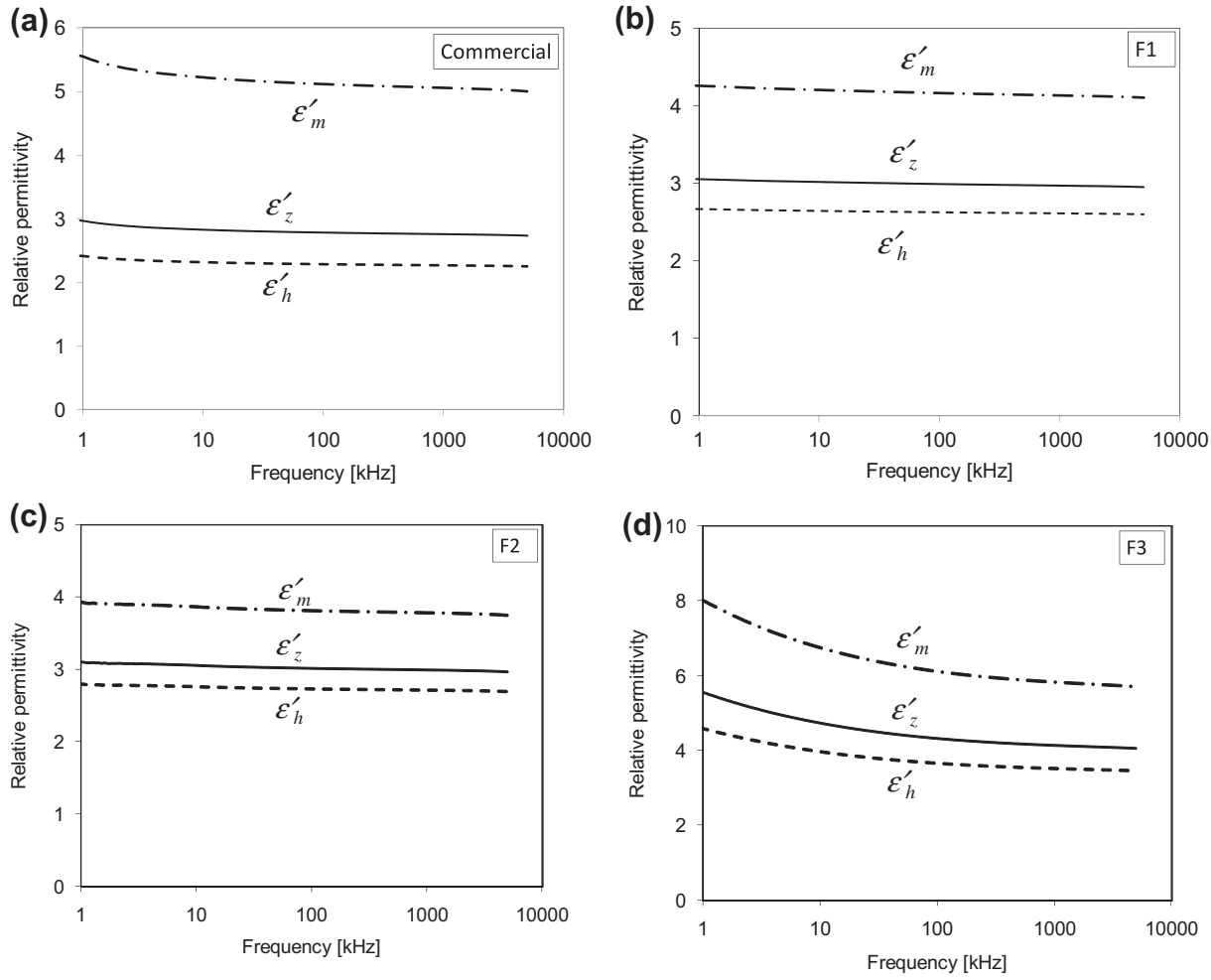

Fig. 14. Frequency spectra of the real parts of the relative permittivity of the aluminium oxide realizing the membrane (ε'_m), the AAO membrane along the direction orthogonal to the pore axis (ε'_h), the AAO membrane along the pore axis (ε'_z), for a commercial membrane and the templates of type F1, F2, F3 of Table 1.

that for F2 there may be an increasing contribution of surface conduction along the pore walls. This conjecture may be confirmed by observing the behaviour of the F3 membrane. Its conductivity, as that of F1, is essentially independent on the electric stress. The fact that the conductivity values for F3 are the highest among all systems could be attributed either to the contribution of a larger carrier density and mobility by the sulphur and water incorporated into the "bulk" of the template or to a larger surface conduction along the pores walls. However, the existence of a significant correlation between the dc conductivity and the pore density is put in evidence in Fig. 9. It can be observed that the conductivity increases linearly (note that the quantities are reported on a log–log plot) with the pore density and the coefficient of determination R^2, providing a measure of how well the linear regression fits the data, is very close to unity. Similar correlation have been attempted also between conductivity and the other morphological characteristics, as pore diameter D and "surface filling factor" D/B in Table 1, but the quality of the rapport has turned out to be quite poor. Therefore it seems reasonable that the main contribution to conduction for all membrane types is mainly along the surface of the pores.

In general, the increase in conductivity in interfacial regions can be attributed to two effects, the existence of lattice defects caused by the structural mismatch or the formation of a space charge region with an increased concentration of mobile point defects [20]. However, in the present analysis, due to the quite low value of the field applied to the membranes, the first mechanism seems to be more plausible.

3.3. Low frequency permittivity and electrical conductivity

At first the measured effective permittivity of the AAO membrane are reported as function of the frequency in the range up to 30 MHz. Fig. 10(a) and (b) shows the spectra of ε'_z and σ_z for a commercial membrane, before and after some thermal cycles. The first heating process has been performed in oven at temperature of 60 °C for 24 h. The second and the last heating treatment of the sample have been carried out at the temperature of 100 °C for 24 h. The sample shows a dispersive behaviour before the heating process due to the effect of humidity [19]. Only after the third thermal process ε'_z becomes quite constant with a value of nearly 2.9 over all the considered frequency range. The effective ac conductivity σ_z, increasing with frequency due to the contribution of the capacitive current component, varies between 10^{-8} and 10^{-5} S/m.

Next, the electrical properties of membranes of type F1, F2, F3 are shown in Fig. 11(a) and (b). It results that after the thermal treatment, the real parts of the permittivity of the F1- and F2-type membranes are quite constant with an average value of about 3 and 3.2, respectively. The effective conductivity σ_z ranges between 10^{-9} and 10^{-6} S/m. For the F3 membrane, it results that after the same thermal treatment the spectrum of ε'_z is not constant with

frequency, thus revealing the presence of higher water content. As regards σ_z, the results show a variation range between 4×10^{-8}–2×10^{-5} S/m.

3.4. Temperature dependence of dc conductivity and permittivity

Next the effect of temperature on the dc conductivity and permittivity has been investigated. It is worth noting that the dc (and not the effective ac) conductivity has been considered in order to get rid of the effects of the capacitive current contributions. As shown by the plots in Fig. 12, the dc conductivity shows an Arrhenius type dependence characteristic which may be attributed to an ionic conduction mechanism:

$$\sigma_z = \sigma_0 \exp(-E_a/kT) \tag{9}$$

where σ_0 is the conductivity at the reference temperature, E_a is the activation energy, k is the Boltzmann constant and T is the absolute temperature. It can be noted that the membranes F1 and F2, being chemically similar, are characterized by very close values of the activation energy (0.27 and 0.28 eV, respectively). Such values are lower than those of the commercial (0.37 eV) and F3 membrane which is characterized by the highest activation energy (0.48 eV).

The effect of the temperature in the range 30–90 °C on the relative permittivity has also been considered for all templates (Fig. 13). In order to allow a better comparability among the different systems, the value of the relative permittivity at 1 MHz, normalized with respect to the measured one at $T = 90$ °C is reported in Fig. 13 as a function of the temperature. In the considered temperature range the permittivity appears to be well approximated by a linear function. The increase of the permittivity with temperature could be ascribed to the increasing contributions of multiple and competing polarization mechanisms (electronic, ionic, dipolar, space charge) so that a clear correlation to the chemical composition and/or morphological characteristics of the templates cannot be achieved. In any case, from the plots of Fig. 13 the temperature coefficient $\Delta\varepsilon'_z/\Delta T$ can be estimated. The results concerning the temperature coefficient for permittivity together with the activation energies obtained from the dc conductivity for the different membranes are summarised in Table 2. The highest temperature coefficient is found for template F3 which exhibits a value (2.3×10^{-2} °C^{-1}) almost one order of magnitude higher than those pertaining to the other systems. In any case, this value is low enough to allow a favourable behaviour of the AAO templates for the realization of nano-interconnects.

3.5. Extraction by modelling of the permittivity value

The relative permittivity of the aluminium oxide realizing the membrane (ε_m) and the effective relative permittivity in the direction orthogonal to the pore axis (ε_h) are obtained from the measured values of ε_z, applying the model described in Section 2.5. The results obtained for the different types of membranes considered in this study (i.e. commercial, F1, F2, F3) are reported in Fig. 14(a)–(d), respectively.

It is observed that the effective permittivity in the direction orthogonal to the pore axis is always lower that the one associated to the pore direction of about 20%. Moreover, the F1 and F2 membranes are characterized by similar chemical content (including especially low water content and phosphorus element) and values of effective permittivity along both directions, parallel and orthogonal to the pore axis, ranging between 2.6 and 3.2. The F3 membranes show smaller pores, higher water content and include sulphur element, as well as a higher effective permittivity, which assume the values of 4 and 3.45, respectively in case of electric field applied along the z- or x-axes. Considering that all F1, F2 and F3 are characterized by nearly the same value of filling factor (as shown in Table 1), it is concluded that the different anodizing conditions (in particular the type of solution and the applied voltage) induce different chemical contents and microstructure of the AAO templates, finally responsible for the different dielectric characteristics of the porous materials.

4. Conclusions

In this work we present a detailed characterization of the low-frequency electrical properties of different families of AAO membranes, considering the effect of the electric field polarization and temperature. A standard test method has been combined with a modelling approach based on the effective medium theory in order to obtain the values of the effective permittivity and electrical conductivity of the anisotropic material along both the directions parallel and orthogonal to the pore axis. This is of particular relevance for application of AAO membranes as template in carbon nanotube interconnects.

The main results of this study are that the tested AAO membranes exhibit values of the relative permittivity around 3, thus making feasible their use as dielectrics in next-generation integrated circuit. In particular the effective permittivity along the pore axis in always greater that the one in the direction orthogonal to the pore of about 20%. It is confirmed that the water content in the membrane increases both its permittivity and electrical conductivity, in particular at lower frequencies.

The conductivity of the membranes increases with the pore density. However, the obtained values are well below those of the conducting nanostructures which should be grown inside the pores to be used in next-generation nano-interconnects.

It is also observed that the anodizing conditions (in particular the type of solution used and the applied voltage) affect sensibly the microstructure and the chemical composition of the AAO templates, and consequently the values of effective permittivity of the resulting porous material. Moreover, the permittivity and conductivity of the AAO membranes exhibit good stability with temperature up to 110 °C, which is also important to avoid variations of the performances in real operating conditions.

Acknowledgment

This work has been performed within the European Research Project CATHERINE – Carbon nAnotube Technology for High-speed nExt-geneRation nano-InterconNEcts – under Grant Agreement No. 216215.

References

[1] M.E. Davis, Nature 417 (2002) 813–821.
[2] S. Shingubara, J. Nanopart. Res. 5 (2003) 17–30.
[3] J.Y. Wan, N. Kulkarni, C.K. Shih, Z. Yao, Appl. Phys. Lett. 84 (7) (2004) 1177–1179.
[4] T. Peng, H. Yang, K. Dai, X. Pu, K. Hirao, Chem. Phys. Lett. 379 (2003) 432–436.
[5] X. Wang, G.R. Han, Microelectron. Eng. 66 (2003) 166–170.
[6] D. Gershon, J.P. Calame, A. Birnboim, J. Appl. Phys. 89 (2001) 8117.
[7] F. Le Coz, L. Arurault, S. Fontorbes, V. Vilar, L. Datas, P. Winterton, Surf. Interface Anal. 42 (2010) 227–233.
[8] P. Ciambelli, L. Arurault, M. Sarno, S. Fontorbes, C. Leone, L. Datas, D. Sannino, P. Lenormand, S. Le Blond Du Plouy, Nanotechnology 22 (2011) 265613 (12p).
[9] ASTM D150 – 98(2004) Standard Test Methods for AC Loss Characteristics and Permittivity (Dielectric Constant) of Solid Electrical Insulation, ASTM International, West Conshohocken, PA. doi:10.1520/D0150-98R04.
[10] I.M.A. Farag, I.K. Battisha, M.M. El-Rafaay, Indian J. Pure Appl. Phys. 43 (2005) 446–458.
[11] D. Cioranescu, P. Donato, An Introduction to Homogenization, Oxford University Press, 1999.
[12] A. Shivola, I.V. Lindell, J. Electromagn. Waves Appl. 4 (1) (1990) 1–26.
[13] A. Sihvola, IEEE N.Y. IEE Electromagn. Waves Ser. 47 (1999).
[14] B. Sareni, L. Krahenbuhl, A. Beroual, A. Nicolas, IEEE Trans. Magn. 33 (2) (1997) 1580–1583.
[15] A.D. Yaghjian, Proc. IEEE 68 (2) (1980) 248–263.

[16] F.J. Garcia-Vidal, J.M. Pitarke, J.B. Pendry, Phys. Rev. Lett. 78 (1997) 4289.
[17] M.E. Mata-Zamora, J.M. Saniger, Rev. Mex. Fis. 51 (5) (2005) 502–509.
[18] R. Morrell, Handbook of Properties of Technical & Engineering Ceramics, Part 2 Data Reviews, Sect. I, High Alumina Ceramics, Her Majesty's Stationery Office, 1987, p. 255.
[19] J. Mollá, M. González, R. Vila, A. Ibarra, J. Appl. Phys. 85 (1999) 1727.
[20] A. Peters, C. Korte, D. Hesse, N. Zakharov, J. Janek, Solid State Ionics 178 (2007) 67–76.